Temperature and humidity sounding from GEO by millimetre-submillimetre wave radiometry

Bizzarro Bizzarri, Alberto Mugnai and Sabrina Pinori

Consiglio Nazionale delle Ricerche (CNR)
Istituto di Scienze dell'Atmosfera e del Clima (ISAC), Sezione di Roma
Via del Fosso del Cavaliere, 100 - I-00133 Roma, Italy

Contact: s.pinori@isac.cnr.it

Extracted from the Final Report of study contract EUM/CO/04/1386/KJG:

"Simulations and User Requirements Review for Precipitating Clouds from Geostationary Orbits in Mm/Sub-mm Bands (GeoRain)"

EUMETSAT responsible: Jochen Grandell
CNR-ISAC responsible: Bizzarro Bizzarri

29 December 2005

PAGE INTENTIONALLY LEFT BLANK

Index

PAGE INTENTIONALLY LEFT BLANK

1. Introduction

1.1 Background on the GOMAS project

The reference system configuration for the study is GOMAS (Geostationary Observatory for Microwave Atmospheric Sounding).

In order to overcome the problem of antenna size corresponding to acceptable resolution, GOMAS exploits very high frequencies. The target resolution of 10 km at the s.s.p. from geostationary orbit is achieved at frequencies as high as 425 GHz by an antenna of 3-m diameter. At this sort of frequencies the water vapour continuum prevents observing the lower troposphere, and also the sensitivity to liquid water is scarce; therefore, lower frequencies are to be used contextually. In GOMAS, the lowest frequency channels are in the oxygen band around 54 GHz, used by AMSU-A for temperature profiling. Moving to higher frequencies, the next oxygen absorption band is at around 118 GHz, where the lower troposphere is well observed, the sensitivity to liquid water decreases whilst sensitivity to ice water and to drop size increases, so that ratioing profiles from the 54 and 118 GHz bands enables deriving cloud microphysical properties correlated to precipitation. The next absorption band is from water vapour, at 183 GHz, used by AMSU-B and MHS for water vapour profiling through the whole troposphere. Sensitivity to ice water further increases, and the information on the vertical water vapour structure contributes to characterise the atmospheric environment backing the precipitation process. A second water vapour band at 380 GHz further augments the differential information in respect of microphysical parameters connected to the precipitation process. The reason for using absorption bands instead of atmospheric windows is that, given the low penetration of high frequencies, the differential information carried out by window measurements would be insignificant whereas absorption bands carry into the retrieval system information on the atmospheric thermo-dynamical situation, that better constrain the possible solution. ***Table 1*** records the bands and channels currently envisaged for GOMAS, for a total up to 44 channels. The IFOV at s.s.p. corresponding to the 3-m antenna diameter is recorded, as well as the expected radiometric accuracy (NEΔT) after averaging the signal over a convenient pixel array so as to achieve SNR $\geq$ 100, that is what is generally required for retrieving vertical profiles. The Incremental Weighting Function (IWF, same shape as the weighting functions) of the channels are shown in ***Fig. 1***.

Table 1 – Radiometric performance assessment for 15 min observing cycle (from Bizzarri et al. 2002)

NEΔT compliance code	Compliant	Nearly compliant	Compliant on 2 Δx or 1 h	Candidate to be dropped

ν (GHz)	$\Delta\nu$ (MHz)	Product resolution	IFOV s.s.p.	Required NEΔT (K)	Expected NEΔT (K)	Peak of IWF	ν (GHz)	$\Delta\nu$ (MHz)	Product resolution	IFOV s.s.p.	Required NEΔT (K)	Expected NEΔT (K)	Peak of IWF
56.325	50	6 x 6 pixels (60 km)	81 km	0.6	0.15	27 km	183.310 ± 0.300	300	2 x 2 (20 km)	24 km	0.6	0.45	10 km
56.215	50			0.5	0.15	23 km	183.310 ± 0.900	500			0.6	0.35	8.5 km
56.025	250			0.5	0.07	17 km	183.310 ± 1.650	700			0.5	0.29	7 km
55.520	180			0.4	0.08	13 km	183.310 ± 3.000	1000			0.3	0.24	6 km
54.950	300			0.4	0.06	10 km	183.310 ± 5.000	2000			0.4	0.17	5 km
54.400	220			0.3	0.07	8 km	183.310 ± 7.000	2000			0.6	0.17	4 km
53.845	190			0.3	0.08	5 km	183.310 ± 17.000	4000			0.3	0.18	surface
53.290	360			0.3	0.06	3 km	380.197 ± 0.045	30	2 x 2 pixels (20 km)	12 km	0.3	2.36	15 km
52.825	300			0.2	0.06	2 km	380.197 ± 0.400	200			0.5	0.91	13 km
51.760	400			0.1	0.05	1 km	380.197 ± 1.500	500			0.5	0.58	11 km
50.300	180			0.1	0.08	surface	380.197 ± 4.000	900			0.5	0.43	9 km
118.750 ± 0.018	6	3 x 3 pixels (30 km)	37 km	0.5	1.32	34 km	380.197 ± 9.000	2000			0.4	0.29	7 km
118.750 ± 0.035	12			0.6	0.93	29 km	380.197 ± 18.000	2000			0.3	0.36	6 km
118.750 ± 0.080	20			0.6	0.72	24 km	424.763 ± 0.030	10	3 x 3 pixels (30 km)	10 km	0.5	3.40	34 km
118.750 ± 0.200	100			0.5	0.32	19 km	424.763 ± 0.070	20			0.6	2.41	28 km
118.750 ± 0.400	200			0.5	0.23	15 km	424.763 ± 0.150	60			0.6	1.39	23 km
118.750 ± 0.700	400			0.5	0.16	12 km	424.763 ± 0.300	100			0.5	1.08	18 km
118.750 ± 1.100	400			0.4	0.16	9 km	424.763 ± 0.600	200			0.5	0.76	15 km
118.750 ± 1.500	400			0.4	0.16	7 km	424.763 ± 1.000	400			0.5	0.54	12 km
118.750 ± 2.100	800			0.3	0.11	5 km	424.763 ± 1.500	600			0.5	0.44	8 km
118.750 ± 3.000	1000			0.2	0.10	3 km	424.763 ± 4.000	1000			0.4	0.34	5 km
118.750 ± 5.000	2000			0.1	0.07	surface	340	8000	1 pixel (10 km)	13 km	1.0	0.30	4 km
							380.197 ± 18.000	2000		12 km	1.0	0.72	6 km
							424.763 ± 4.000	1000		10 km	1.0	1.02	5 km

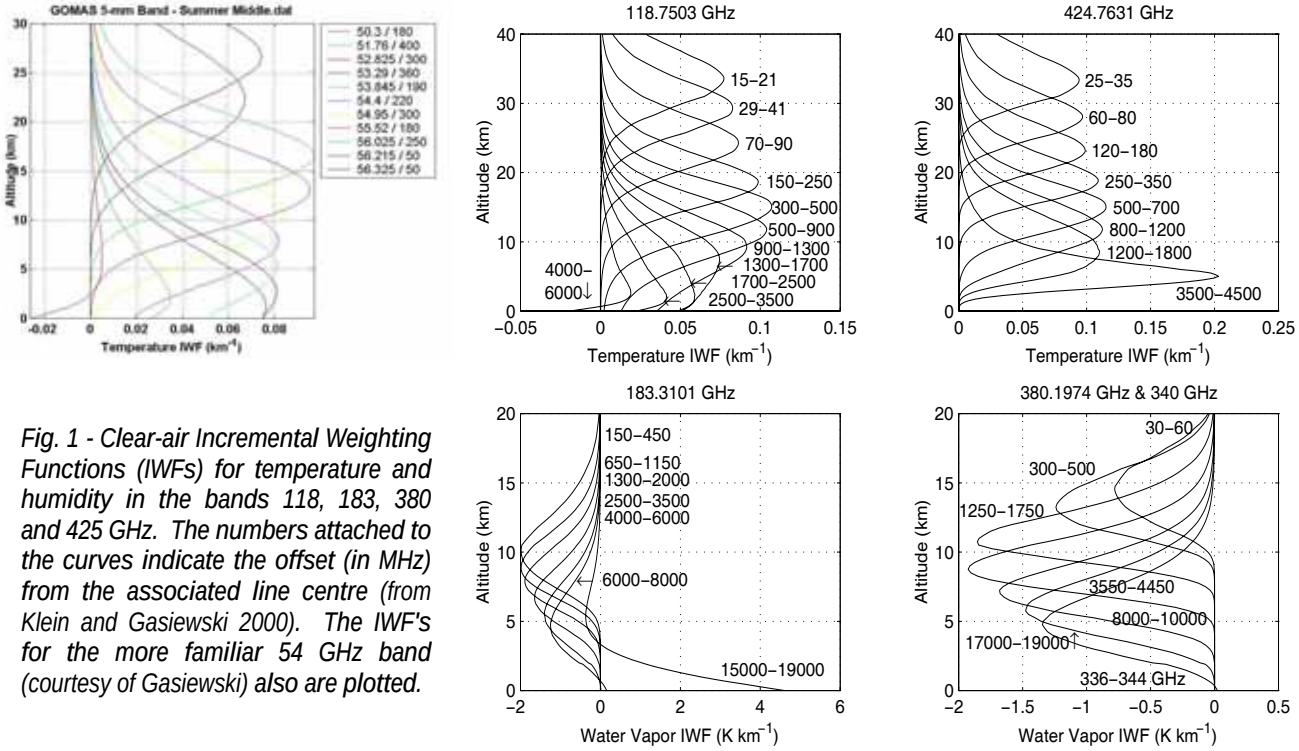

Fig. 1 - Clear-air Incremental Weighting Functions (IWFs) for temperature and humidity in the bands 118, 183, 380 and 425 GHz. The numbers attached to the curves indicate the offset (in MHz) from the associated line centre (from Klein and Gasiewski 2000). The IWF's for the more familiar 54 GHz band (courtesy of Gasiewski) also are plotted.

1.2 Purpose of the study

The principle of measuring precipitation from GEO is to exploit the perturbation induced by clouds and precipitation on the temperature and humidity profiles measured by using different absorption bands where the impact of liquid or ice water, drop or crystal concentration and size distribution and ultimately precipitation is different. However, profiles retrieved by using different bands have a background intrinsic difference (i.e., give different retrievals even in the absence of clouds) because of the different structures of the weighting functions. For example, retrievals from the highest frequency bands are inaccurate or blind to the lower troposphere, as clearly shown by Fig. 1. The first purpose of the study is to assess these background differences before introducing the perturbation of clouds and precipitation.

There is also a second purpose. By combining retrievals from different bands, the best clear-air temperature and humidity profiles can be obtained. Currently there is no consensus on the usefulness of these profiles since, in the MW range, the vertical resolution cannot be very good, thus the output of NWP could be competitive. However, the contribution of the highest frequency bands could improve the quality of sounding from GEO as compared to that one from AMSU in the upper troposphere, and anyway the high repeat cycle could turn out to be very useful when assimilated in mesoscale NWP models. An example of early exercise on the subject of clear-air temperature-humidity profile from the GOMAS frequencies (not including the 54 GHz band) is shown in ***Fig. 2***, from Blackwell and Staelin 1996. It is noted that the GOMAS bands/channels are identical to those of the equivalent American project, GEM (Geostationary Microwave observatory).

Once the clear-air temperature and humidity profiles are characterised, the next step is to appreciate how cloud interference progressively degrades the profiling capability, i.e. to which extent temperature/humidity sounding by millimetre-submillimetre wavelengths from GEO can be considered "all-weather". Obviously, in the presence of heavy precipitation the weighting functions are flattened towards the cloud top, therefore profiling becomes impossible. However, it is important to assess how close to precipitating cores profiling is still significant. In fact, the alternative to measure precipitation is to derive it by 4-D assimilation of frequent sounding.

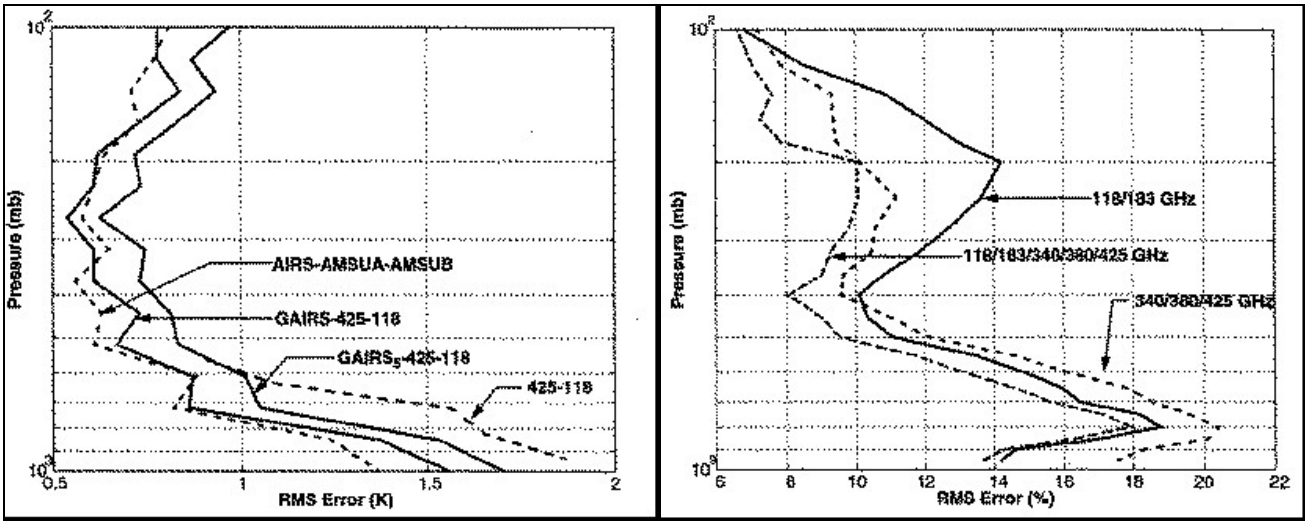

Fig. 2 – Retrieval errors for bands 118, 183, 380, and 425 GHz, stand-alone or associated with an IR sounder of the IASI or AIRS class ("GAIRS"). Temperature is shown on the left hand, and humidity on the right. On the left hand, GAIRS + 118 + 425 is compared to GAIRS alone and to 118 + 425 alone. For reference, the EOS/Aqua AIRS + AMSU/A + AMSU/B complex also is shown (from Blackwell and Staelin 1996).

1.3 Structure of the study

Fig. 3 deploys the architecture for the first step, clear-air temperature-humidity sounding.

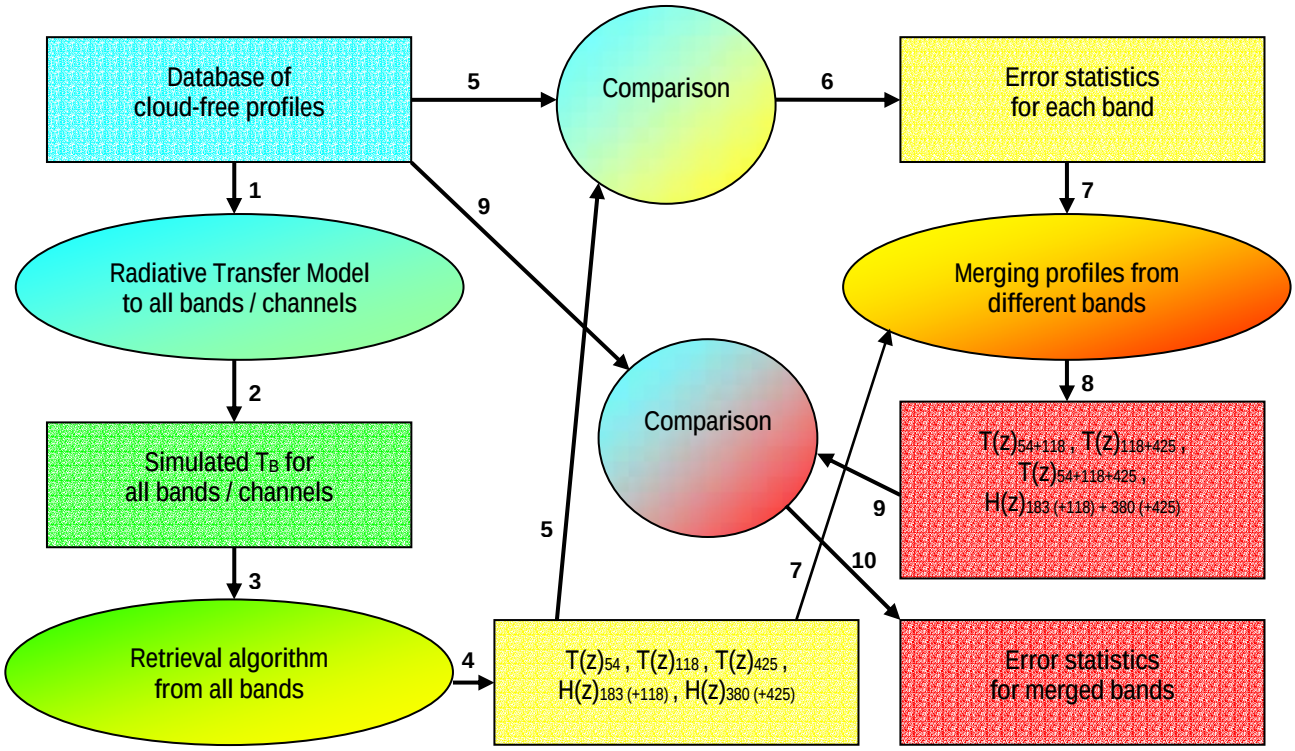

Fig. 3 – Architecture of the study for clear-air temperature-humidity profile characterisation.

The starting point is to collect a database of temperature-humidity profiles and select those that can be classified as "cloud-free". A Radiative Transfer Model (RTM) applied to the profile simulates the brightness temperature in the various GOMAS channels (up to 44, see Table 1). A retrieval algorithm is

applied to each set of channels of a band, and profiles are generated. From the three oxygen bands (54, 118 and 425 GHz) three independent profiles are retrieved, with different error structure due to the different sensitivity of the channels to the atmospheric layer (see the IWF in Fig. 1). Retrieval of water vapour profiles from the 183 and 380 GHz bands requires support from the closed temperature-sensing band, 118 and 425 GHz respectively, whereas for temperature profiling any reasonable first-guess humidity profile would be sufficient. The retrieved profiles are compared with the initial ones in the database, and error statistics are built for each band. The information on error structures is utilised for synthesising a new profile of temperature and humidity by appropriately merging the various bands.

The next step is to assess the effect of clouds on the brightness temperatures and to observe the departures from the clear-air situation. ***Fig. 4*** deploys the architecture of this second step.

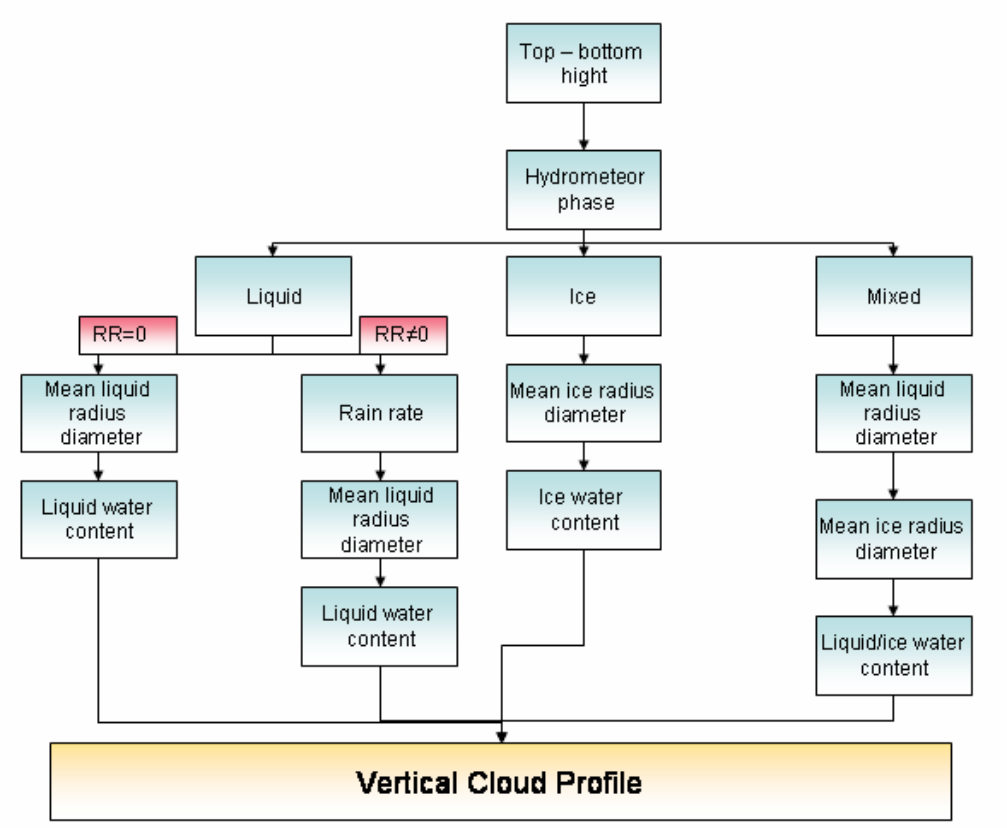

Fig. 4 – Scheme for introducing "disturbing" clouds in the clear-air profile.

The algorithm first input is the clear-air profile, then the cloud 'disturbance' is introduced, defining the following parameters: cloud top and bottom height, phase, mean radius of the hydrometeor, and the liquid/ice water content. Once obtained the vertical profiles, a RTM designed to handle with clouds generates the upwelling T_Bs, to be compared with the initial clear-air ones.

2. Description of the experiment in clear-air

2.1 Profile data set

To study the potentiality of the high frequency channels in retrieving the vertical temperature and humidity profiles a database of radio sounding data has been built. The dataset is composed of radio sounding measurements (from the TEMP file) collected from 15th March to 15th July 2005 collected by five different locations (circles in ***Fig. 5***): Pratica di Mare, Cagliari-Elmas, Trapani-Brigi, Milano-Linate (Italy), and Lindenberg (Germany). The sounding data has been downloaded from the University of Wyoming (U.S.) web site (http://weather.uwyo.edu).

Together with the radio sounding the clear sky information has been retrieved, in order to select only the clear sky profiles. The cloud cover is derived from the SYNOP file, where the information is given using a 1/8 cloud scale, with 0 corresponding to clear sky, and 8 to completely cloudy. The cloud cover data has been extracted from the sounding images available on the Internet on the web page of the University of Cologne (Germany), http://www.meteo.uni-koeln.de.

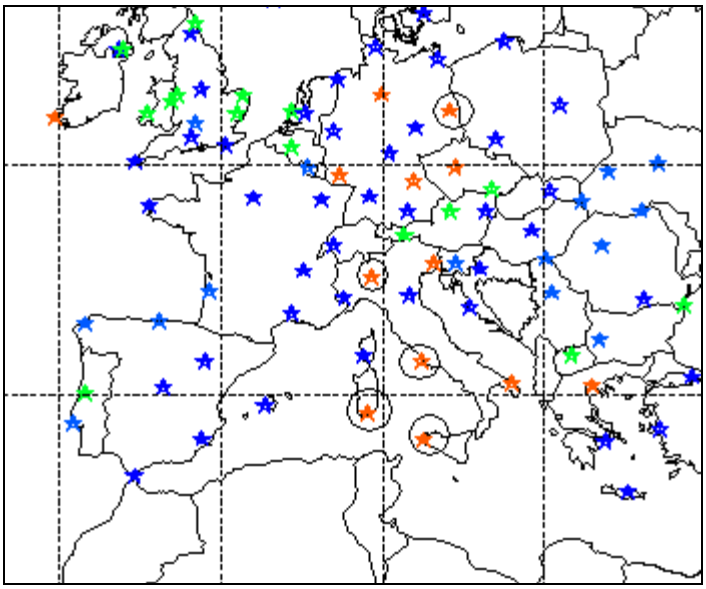

Fig. 5 – Location of sounding measurement (the black circles correspond to the chosen locations).

The first task has been to separate the clear sky profiles from all the measurements (around 3000 measurements) and to build the database. A table with the cloud coverage has been built for every sounding station considered. Then from the entire volume of sounding profiles only the clear-sky ones have been selected considering the location, the date and the time of the measurement. In this way, a datasets of around 200 profiles has been extracted and used to simulated the brightness temperatures at the GEM/GOMAS selected channels (see Table 1).

2.2 Radiative Transfer Models in clear-air

We had three Radiative Transfer Models available for this study:

- MRT (Microwave Radiative Transfer), has been provided to us by Albin Gasiewski, of the NOAA Environmental Technology Laboratory (ETL);
- The RTM developed at the MIT Research Laboratory of Electronics (RLE), mostly by Philip Rosenkranz, for the retrieval of atmospheric temperature and moisture profiles (Rosenkranz 2001);
- 3D-adjusted plane-parallel radiative transfer model described in the studies of Roberti et al. 1994, Liu et al. 1996, Bauer et al. 1998, and currently used at the CNR-ISAC laboratories for studies at high frequencies.

To choose the best RTM for the high frequencies channels took a lot of time beacuse the performances of each RTM have been valuated considering the results of the temperature and humidity retrievals. One of the major problems has been the definition of the surface emissivity, and the final decision has been to compute the T_Bs assuming an ocean surface with a constant surface emissivity of 0.65 for each frequency. Starting from this assumption, we applied the three RTMs to a subset of sounding profiles and the results has been that the RTM that give us the best results in terms of retrieval has been the 3D-adjusted plane-parallel (CNR-ISAC). Then the 3D-adjusted plane-parallel RTM has been applied to the dataset of clear sky profiles.

2.3 Short description of the 3D-adjusted plane-parallel radiative transfer model

In order to simulate the upwelling brightness temperatures (T_Bs) that would be observed by the geostationary radiometer, we apply to the measured radio sounding clear-sky profiles the 3D-adjusted plane-parallel radiative transfer model, RTM. The RTM-generated upwelling T_Bs have been calculated at nadir viewing angle. This RTM has been developed to compute and study the T_Bs of simulated precipitating events, giving a strong accent on the scattering properties of precipitating system, where these properties has been described in full detail. In this case we exploit the capability to compute the absorption of the atmospheric gases and of the water vapor, combined with the surface emissivity model.

The required inputs to the RTM are: suitable temperature / moisture profiles and temperature / emissivity of the surface, as well as vertical profiles of liquid/ice water contents (LWC/IWC) of the various hydrometeors - along with their single-scattering properties. Absorption by atmospheric gases at microwave frequencies are calculated according to the Liebe and Gimmestad 1978 and Liebe 1985 clear-moist air refractivity model that provides a combined water vapor – oxygen volume absorption coefficient.

Surface emissivity is assigned dependent upon frequency and surface characteristics (land/ocean, surface roughness, type of soil and soil cover, soil humidity, etc.). While it can be highly variable depending on these parameters, for this study we assume constant values of 0.9 and 0.65 for land and ocean backgrounds, respectively – see Hewison and English 2000 for the emissivity of many land surfaces. The uncertainty in surface emissivity is taken into account within the Bayesian retrieval scheme developed by Mugnai et al. 2001 and Di Michele et al. 2003. This is accomplished by means of an error covariance matrix, which accounts for T_B sensitivity to parameter uncertainties and approximations used in the forward RTE model (e.g., Tassa et al. 2003).

2.4 Description of the retrieval model utilised (from MIT/ETL)

The MIT retrieval method (Rosenkranz, 2001) is an iterated minimum-variance algorithm retrieval that has been developed for the retrieval of vertical profiles from AMSU data. The retrieval algorithm draws on retrieval methods described in Wang and Chen (1990), Wilheit (1990), Kuo et al. (1994), and Wilheit and Hutchinson (1997). A priori statistics are required for the parameters that characterize the state of the system. Statistical correlations between temperature and relative humidity are not allowed to influence the retrieved profiles. Temperature is retrieved from the oxygen-bands and moisture and surface parameters from the water vapour and window channels. Hence only radiative-transfer influences (e.g. water-vapour continuum absorption and surface emissivity in the oxygen band) link different parameters in the retrieval.

2.4.1 Forward Model

Radiative Transfer Calculations

Planck's equation for radiant intensity is a non-linear function of temperature. For microwave (MW) frequencies, however, the physical temperatures encountered in the Earth's atmosphere lays at the high-temperature asymptote of this function. Hence, brightness temperature can be used as a surrogate for radiance in the equation of radiative transfer with an accuracy of a few hundredths of a Kelvin. The

only exception occurs with the cosmic background, which must be assigned an effective brightness temperature at frequency ν (Janssen, 1993)

$$\Theta_C = (h\nu / 2k)(e^{h\nu/kT_C} + 1)(e^{h\nu/kT_C} - 1)^{-1}$$

instead of its actual temperature $T_C = 2.73$ K in order to linearise the Planck's function.

The radiative transfer equation considered in this algorithm is written in the form

$$\Theta = \Theta_{direct} + \tau[\Theta_S + \Theta_{sky}(1 - \Theta_S / T_S)] \quad (1)$$

where Θ is the brightness temperature emitted from the top of the atmosphere, τ is the one-way transmittance of the atmosphere, Θ_{direct} is the component of the brightness temperature emitted from the atmosphere in a direct path to space, T_S is the surface temperature, Θ_S is the surface brightness temperature, and Θ_{sky} is the sky brightness temperature as it would be observed from the surface.

The atmospheric transmittance τ is computed with the rapid algorithm described in Rosenkranz (1995) and Rosenkranz (1998). The form of Θ equation (1) allows separation of the estimation of surface brightness from estimation of surface brightness temperature.

Surface Brightness Model

The model for the surface combines an a priori emissivity of the surface type with an analytic function which allows the retrieval to adapt the surface brightness temperature to the data. The surface brightness temperature spectrum Θ_S is modelled as

$$\Theta_s = T_S\varepsilon_0 + \frac{R_0T_0 + R(\nu)T_\infty}{R_0 + R(\nu)} \quad (2)$$

where ε_0 is a preliminary estimate of surface emissivity, and R_0 and $R(\nu)$ are defined as

$R_0 = (\nu_0/31.4\ \text{GHz})^S$

$R(\nu) = (\nu/31.4\ \text{GHz})^S$.

The second term of (2) is a smooth four parameter function of frequency (Grody, 1988) which allows for effects such as ocean surface roughness, errors in the dielectric constant model, misclassification of the surface, or errors in the land fraction within a footprint. T_0, T_∞, ν_0 and *S* are parameters defining the curve. *S* is fixed at 1.2 over land or mixed land/water, or 3 over ocean, and treats R_0, T_0, T_∞ as uncorrelated free parameters for which it solves.

For the data used in this work, the only surface types are land and ocean. For land $\varepsilon_0 = 0.95$. For ocean, ε_0 is calculated by a second-order polynomial function of temperature with coefficients fitted to the emissivity of a flat surface viewed at the polarization of the radiometer, which rotates with scan angle. A separate set of these coefficients was pre-computed for each incidence angle and frequency. The model in Lamkaouchi et al. (1997) was used for seawater dielectric constant.

Atmospheric Moisture and Condensation Model

Brightness temperature at the GOMAS frequencies depend on the vertical profile of atmospheric opacity relative to temperature, but do not themselves distinguish, at any given altitude, between opacity and due to the water vapour and opacity due to liquid water. In this part of the work we will make use only of selected clear sky profiles, without cloud liquid water, but it is important to describe also the model properties for the treatment of the atmospheric moisture and the condensation because in other in the following we will investigate the impact of the presence of different types of non-raining clouds on the brightness frequencies and the retrieval capability.

Cloud coverage is parameterised as in the stratiform condensation model of Sundvquist et al. (1989), where a relative humidity threshold determines the onset of condensation. Although the water vapour profile is saturated within the cloudy part of the field of view, it is assumed that the condensation process is not spatially resolved, hence the threshold is less than 100 % relative humidity. Currently the threshold is set to 85 %.

In the condensation model, the vapour and cloud liquid water density profiles are both linked to a single parameter H. When H ≤ 85 %, H is equal to relative humidity; in the range 85 to 115, H changes from a water-vapour variable to liquid-water, and values of H > 115 increase liquid water while the vapour remains at saturation. Because convergence, to be discussed later, is determined from the brightness temperature residuals, which in turn are computed using vapour and liquid column density, the role of H in this algorithm is only to introduce the a priori statistics and constrains. The average vapour density in the field of view is related to H by

$$\rho_v = \begin{cases} \rho_s H/100 & H \le 85 \\ \rho_s[0.85 + 0.15(2b - b^2)] & 85 < H < 115 \\ \rho_s & H \ge 115 \end{cases} \quad (3)$$

and the liquid water density averaged over the field of view is calculated as

$$\rho_L = \begin{cases} 0 & H \le 85 \\ C_L b^2 & 85 < H < 115 \\ C_L(2b-1) & H \ge 115 \end{cases} \quad (4)$$

In the previous equation, b = (H-85)/30, ρ_s is the saturation value of vapour density, and C_L is a coefficient equivalent to a mass mixing ratio of 0.5 g liquid/kg air. The saturation vapour density is computed from the temperature profile. Saturation is calculated with respect to liquid water (by extrapolation) even when the temperature is below 273 K. Thus, the model will allow supercooled liquid water clouds and water vapour greater than the saturation value over ice (but not greater than ρ_s).

2.4.2 Solution method

The input consists of two vectors, a vector of measured brightness temperature and one with the validity of whose elements are either zero or one, this provides a way of handling missing or bad data. The principal steps in the retrieval algorithm are:

1) Based on location and month, choose an *a priori* temperature profile $\hat{T}_0$. At present the *a priori* relative humidity profile is global.
2) Using location or other criteria, classify the surface and compute an *a priori* surface brightness temperature for this class, that will depend on the surface temperature.
3) Test for convergence of the window and water vapour sounding channels brightness temperature. If not converged, update the relative humidity profile and the surface brightness temperature spectrum using these channels.
4) Test for convergence of oxygen sounding channels. If not converged, update the temperature profile using these channels.
5) Return to step 2 if convergence does not occur in step 4; else to step 3 if convergence does not occur in step 3; else exit.

Steps 3) and 4) are described in greater detail in the following sections.

Estimation of surface brightness temperature and atmospheric moisture

The H profile and the three surface brightness temperature parameters R_0,T_0, and T_∞ are concatenated into a vector P. The cost function to be minimized is (see Eyre, 1989)

$$(\hat{P} - \hat{P}_0)^t S_P^{-1} (\hat{P} - \hat{P}_0) + (\Theta^* - \Theta)^t S_e^{-1} (\Theta^* - \Theta) \quad (5)$$

In the previous equation, $\hat{P}$ is the estimate of P, $\hat{P}_0$ is the a priori mean value of P and $\boldsymbol{S}_P$ is its covariance matrix with respect to $\hat{P}_0$, Θ^* is a vector containing the measured brightness temperatures of the window and water vapour sounding channels, $\boldsymbol{S}_e$ is their error covariance matrix, and Θ is a brightness temperature vector computed at each iteration from the current estimated values of

temperature, moisture, and surface brightness, using the forward model. Superscript *t* indicate the transpose.

Given the previous estimate $\hat{P}_{n-1}$ (which is $\hat{P}_0$ on the first iteration), the next estimate of *P* is obtained by Newtonian iteration (Rodgers, 1976), except that Eyre's (Eyre, 1989) method of damping is used to avoid large relative humidity increments because of the non-linearity of the problem

$$\hat{P}_n = \hat{P}_{n-1} - \delta[\hat{P}_{n-1} - \hat{P}_0] + \delta S_P W_P^t X_P \qquad (6)$$

in which XP is the solution vector to

$$[W_P \delta S_P W_P^t + S_e] X_P = \Theta^* - \Theta - \Theta' + W_P \delta[\hat{P}_{n-1} - \hat{P}_0] \qquad (7)$$

where Θ' is a possible correction (presently zero) to adjust for transmittance-model errors, and $\boldsymbol{W}_p$ is a Jacobian matrix (matrix of derivatives of Θ with respect to *P*), which is computed for the state represented by $\hat{P}_{n-1}$ (the forward model is assumed to be linearizable within the retrieval error space). The damping factor is:

$$\delta = \begin{cases} 1 \\ 0.1 \end{cases}$$

where δ is a scalar rather than a matrix as in (Eyre, 1989).

The parts of $\hat{P}_0$ and $\boldsymbol{S}_P$ corresponding to relative humidity were calculated from the TIGR profile ensemble (Chedin et al., 1985). For the surface parts, it is necessary postulate statistics based on physical considerations and previously observed ranges of variation. Mean values are set to

R_0 = 3.5 (land or mixed) or 2.1 (water)

T_0 = 0

T_∞ = 0

and variances are set to

S_{R_0} = 2.25

S_{T_0} (Kelvin)^2 = 100 (land) or 9 (water)

S_{T_∞} (Kelvin)^2 = 100 (land) or 25 (water)

For the moisture channels, the measurements error covariance $\boldsymbol{S}_e$ is the sum of contributions due to the expected instrument noise (see Table 1) plus a diagonal error of (1.5 K)^2 , which approximately represents errors in Θ resulting from errors in the temperature profile retrieval.

After update of $\hat{P}$ by (6), the water vapour and liquid water profiles are computed from (3) and (4), and surface brightness is computed for both window and sounding frequencies from (2), using the new estimate. If the estimated vapour mixing ratio at any level is less than 10^{-3} g/kg it is set to that minimum value.

Estimation of the temperature profile

Although done separately in step 4), the estimation of temperature uses essentially the same equations as for the moisture, but with T replacing P everywhere and with no damping (δ = 1). The atmospheric temperature vector is augmented by T_S, which is considered to be distinct from the air temperature near the surface. A cost function of the form of (5), with P replaced by T is to be minimized separately for the temperature profile. Given an existing estimate $\hat{T}_{n-1}$, the next estimated profile is determined from a vector Θ* of observed brightness temperature for all the oxygen sounding channels. However, the updated surface temperature is not allowed to become less than the estimated surface brightness temperature $\hat{\Theta}_S$. In (6) and (7), $\boldsymbol{W}_p$ is replaced by $\boldsymbol{W}_T$, the Jacobian matrix of derivatives of Θ with respect to T evaluated at $\hat{T}_{n-1}$. The error covariance matrix $\boldsymbol{S}_e$ includes uncertainties due to surface

brightness, water vapour, liquid water, and the instrument noise. The covariance of the atmospheric temperature vector was computed from the TIGR ensemble (Chedin et al., 1985). To account for differences between T_S and the air temperature near the surface (T_{1013}), the variance of T_S is set to a value of 16 K, twice larger than the variance of T_{1013}, but its mean and covariances with other levels are equal to those of T_{1013}. Hence, the correlation coefficient of T_S with other levels is smaller than that of T_{1013} with those levels.

Convergence tests

Convergence is tested separately for the temperature channels in step 4) and for the moisture/surface channels in step 3). Iteration of either step is suspended when one of the following condition is met:

- the computed brightness temperature vector Θ meets the noise closure criterion

$$\sum_{i=1}^{N_B} [\Theta_i^* - \Theta_i - \Theta_i^{'}]^2 \, \Delta T^{-2} \le N_B \qquad (8)$$

  where ΔT_i is the instrument noise (not the total measurement error) on channel i and N_B is the number of valid elements in Θ*; or
- when successive computation of the left side of (8) change by less than 1 % for temperature or 2 % for moisture/surface channels; or
- when the number of iterations exceeds a preset limit (currently 12 for the temperature channels and 16 for the moisture/surface channels).

Typically, iteration of the temperature profile ceases after one or two iterations, but the moisture profile often requires six or more iterations.

Performances of the retrieval algorithm with AMSU-A and AMSU-B data are shown in Rosenkranz 2001. The retrieval presents good performances for clear-air footprints, while precipitating areas are still not well treated. Future developments of this algorithm will be directed toward improvements in the surface model and the incorporation of precipitation flags and/or corrections.

3. Presentation of the results in clear-air

3.1 Retrieval of temperature and humidity: some examples

Once the dataset of clear sky has been produced, the 3-D adjusted plane parallel RTM has been applied to the radiosonde profiles, and the MIT retrieval algorithm developed by Philip Rosenkranz has been applied to the simulated brightness temperature to retrieve back the profiles. In ***Fig. 6*** and ***Fig. 7*** temperature and dew-point profiles retrieved and measured are compared. The first-guess profiles used by the retrieval are also shown in the figures. As expected, the retrieved profiles are fairly smooth curves, without the fine vertical structure of the radiosonde. These retrievals have been done using the 118 and 183 GHz bands, using the 118.75±5.00 GHz as window channel.

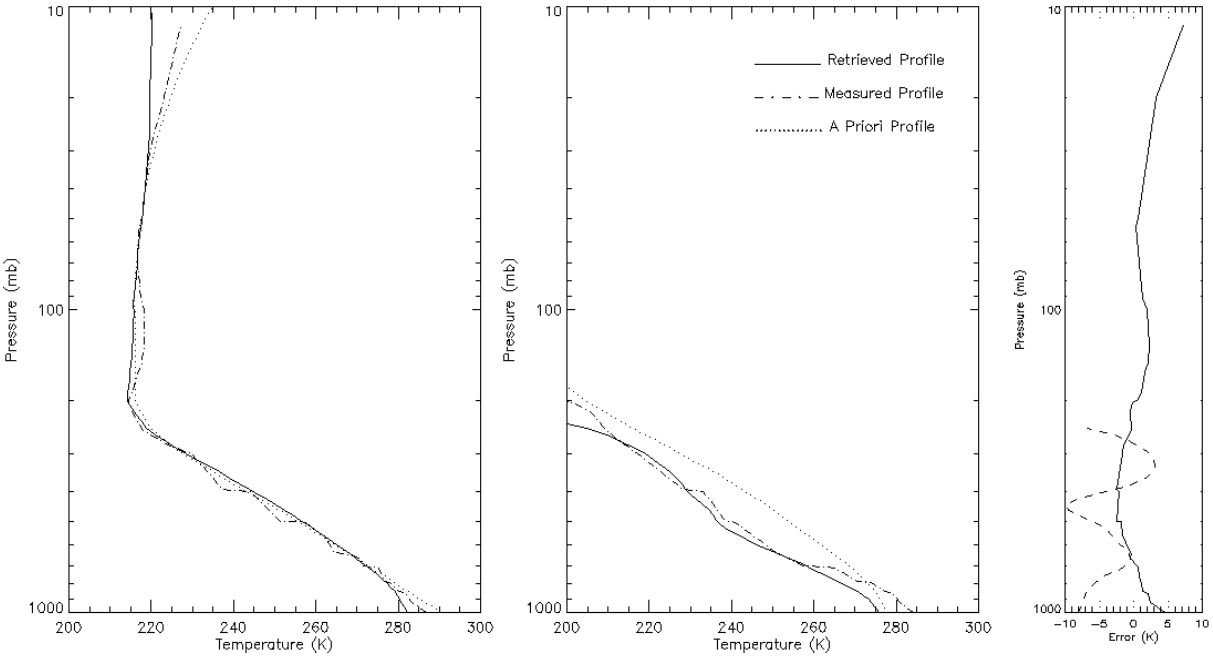

Fig. 6 – Retrieval versus radiosonde profiles at Milano Linate (Italy), on 15 May 2005 at 00 UTC. In the right panel the retrieval errors are show (temperature solid line, dew-point dashed line).

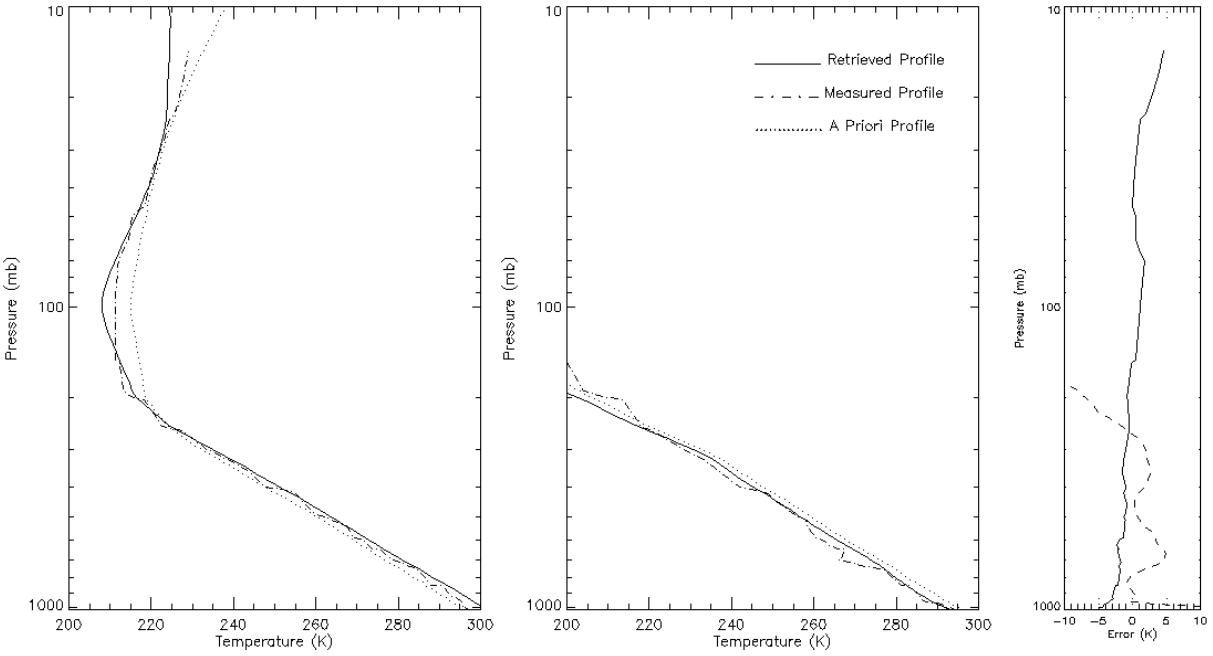

Fig. 7 – Retrieval versus radiosonde profiles at Pratica di Mare (Italy), on 23 June 2005 at 00 UTC. In the right panel the retrieval errors are show (temperature solid line, dew-point dashed line).

With the 183 GHz band, the weighting function of the most absorbing channel peaks around 300 hPa, consequently the dew-point errors are larger at higher altitudes. These are only two examples of the retrieval performances.

3.2 Temperature profile retrieval performances

At this point, the retrieval algorithm has been applied to the entire dataset, using different bands or bands combinations. ***Fig. 8*** and ***Fig. 9*** report the standard deviation of errors (true - retrieved profile) for retrievals from single bands (54, 118 and 425) and combined bands (54 + 118, 118 + 425 and 54 + 118 + 425 GHz) respectively.

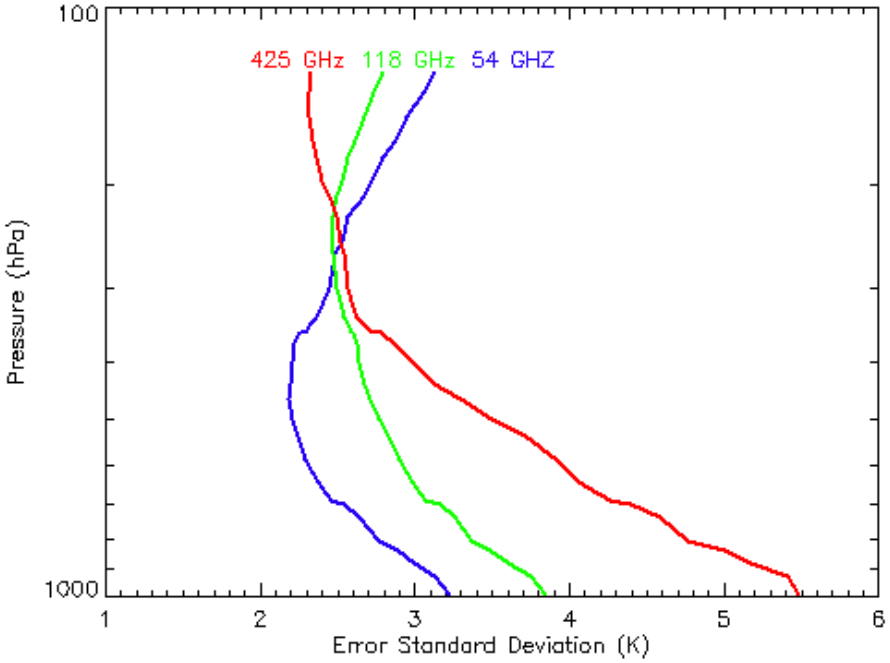

Fig. 8 – Standard deviation of retrievals from the three O_2 bands as stand alone.

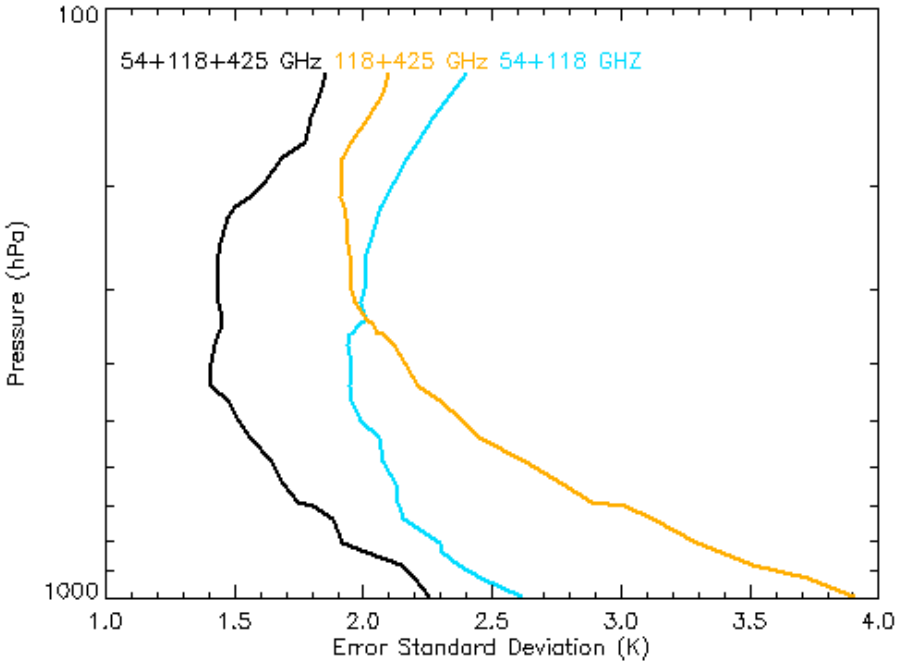

Fig. 9 – Standard deviation of retrievals from different combinations of the three O_2 bands.

From Fig. 8 it is easily observed that the 54 GHz band has highest performances in the low-mid troposphere, up to 280 hPa. In this same layer, 118 performs better that 425 GHz. Above 280 hPa, both 118 and 425 GHz perform better than 54 GHz, and 425 performs better than 118 GHz. As regards band combinations, the couple 118 + 425 GHz performs better than the couple 54 + 118 GHz above 350 hPa. However, the most important result is that the combination of the three bands (54 + 118 + 425) has much higher performance, with accuracy reaching as much as 1.5 K in the middle troposphere.

3.3 Humidity profile retrieval performances

Fig. 10 reports the results for water vapour bands: 183 GHz (with support from 118 GHz for temperature information), 380 GHz (with support from 425 GHz and the window at 340 GHz) and the combination 183+118 and 380 + 425 GHz.

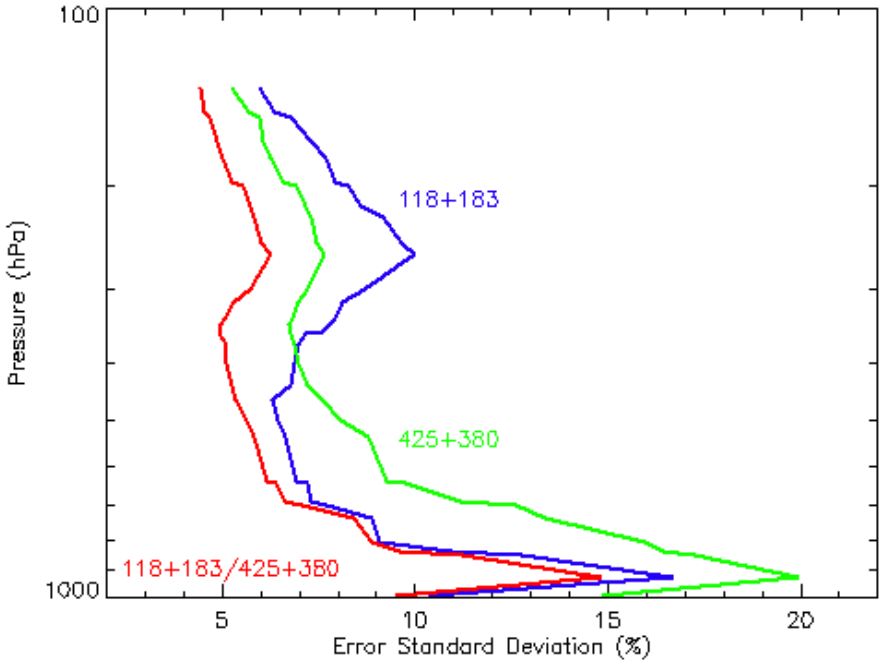

Fig. 10 – Standard deviation of retrievals of relative humidity from stand-alone or coupled water vapor bands.

It can be observed that 183 GHz performs better for altitudes up to 400 hPa, then 380 GHz prevails. The combination of the two bands provides very good performance, better than 10 % above 800 hPa with peak of 5 % in the middle-high troposphere.

4. Experiments of cloud perturbation

4.1 Description of the experiment

The ultimate purpose of this study would be to determine to which extent the temperature and humidity profiles from GOMAS bands can be considered "all-weather", i.e. how close to precipitating cores it is possible to retrieve vertical profiles. To this purpose, we now start "perturbing" clear air profiles by inserting controlled cloud types.

The database of clear-air profiles built for the clear-air experiment is used as starting point for the study of the cloud 'disturbances'. The different clear-air profiles (and the corresponding Brightness Temperatures, T_Bs) have been selected to be used as '*reference*' for the initial study of the cloud impact on the atmospheric column.

Three cloud types have been selected for the experiment:

1) Cirrus cloud;
2) Marine (thin) stratus cloud;
3) Thick stratus, or nimbus-stratus, possibly precipitating (e.g., monsoon).

The different cloud characteristics have been selected from literature. ***Table 2*** records the values of the different variables chosen to describe the clouds: thickness, liquid and/or frozen water content, cloud phase and mean particle radius.

Table 2 - Principal characteristic of the cloud types considered

Cloud type	Cloud bottom – top (thickness) [km]	Phase	Liquid water content [g/m³]	Ice water content [g/m³]	Mean radius [μm]	Reference
Cirrus	8.3 – 8.6 (0.3)	Ice	-	0.03	-	Rogers and Yau 1996
Marine stratus	0.7 – 1.8 (1.1)	Liquid	0.25	-	18	Telford and Wagner 1981
Nimbus-stratus	2.0 – 8.5 (6.5)	Mix	1.4	1.4	1000	Wang 2005, Shaw 2003

The procedure to compute cloud profiles along the vertical, shown in Fig. 4, and the follow-on computation of brightness temperatures at the GOMAS frequencies, have been performed by means of the MRT (Microwave Radiative Transfer) code provided to us by Albin Gasiewski (NOAA/ETL), an updated version of the original Klein and Gasiewski 2000. Constant emissivity over ocean ($\varepsilon = 0.53$) was used. The 'perturbed' T_Bs were compared with those for clear-air.

4.2 Analysed cases

The study has evaluated the impact of changing cloud parameters, as follows:

- ***case 1***: variation of cirrus IWC (Ice Water Content), in three steps: 0.03 g/m^3, 0.09 g/m^3, 0.20 g/m^3;
- ***case 2***: variation of cirrus thickness: 0.3 km, 0.6 km, 0.9 km;
- ***case 3***: variation of marine stratus LWC (Liquid Water Content): 0.25 g/m^3, 0.50 g/m^3, 0.75 g/m^3;
- ***case 4***: variation of marine stratus thickness: 1.1 km, 1.4 km, 1.7 km;
- ***case 5***: variation of nimbus-stratus LWC (Liquid Water Content): 0.6 g/m^3, 1.2 g/m^3, 2.4 g/m^3;
- ***case 6***: variation of nimbus-stratus thickness: 2.5 km, 4.5 km, 6.5 km.

5. Presentation of the results of cloud perturbation experiments

5.1 Cirrus clouds

Fig. 11 and ***Fig. 12*** show the T_Bs of case 1 and case 2 respectively for every frequency grouped by bands. Fig. 11 refers to changes of IWC, Fig. 12 to variation of thickness. In both cases we can see that the lower frequencies (54 and 118 GHz bands) are not sensitive to variation of both IWC and thickness of the cirrus cloud. We can expect this behaviour because the cirrus ice crystals are very thin and do not scatter at these frequencies. On the contrary, the high frequencies (380 and 424 GHz bands) are sensitive in variation of the IWC with T_Bs differences from the clear-air of 10-20 K. Also the 183 GHz band is affected by variations of the cirrus thickness, but in this case it is due to variation of the water vapour profile. The high frequencies are also weakly sensitive to variation in the cloud thickness.

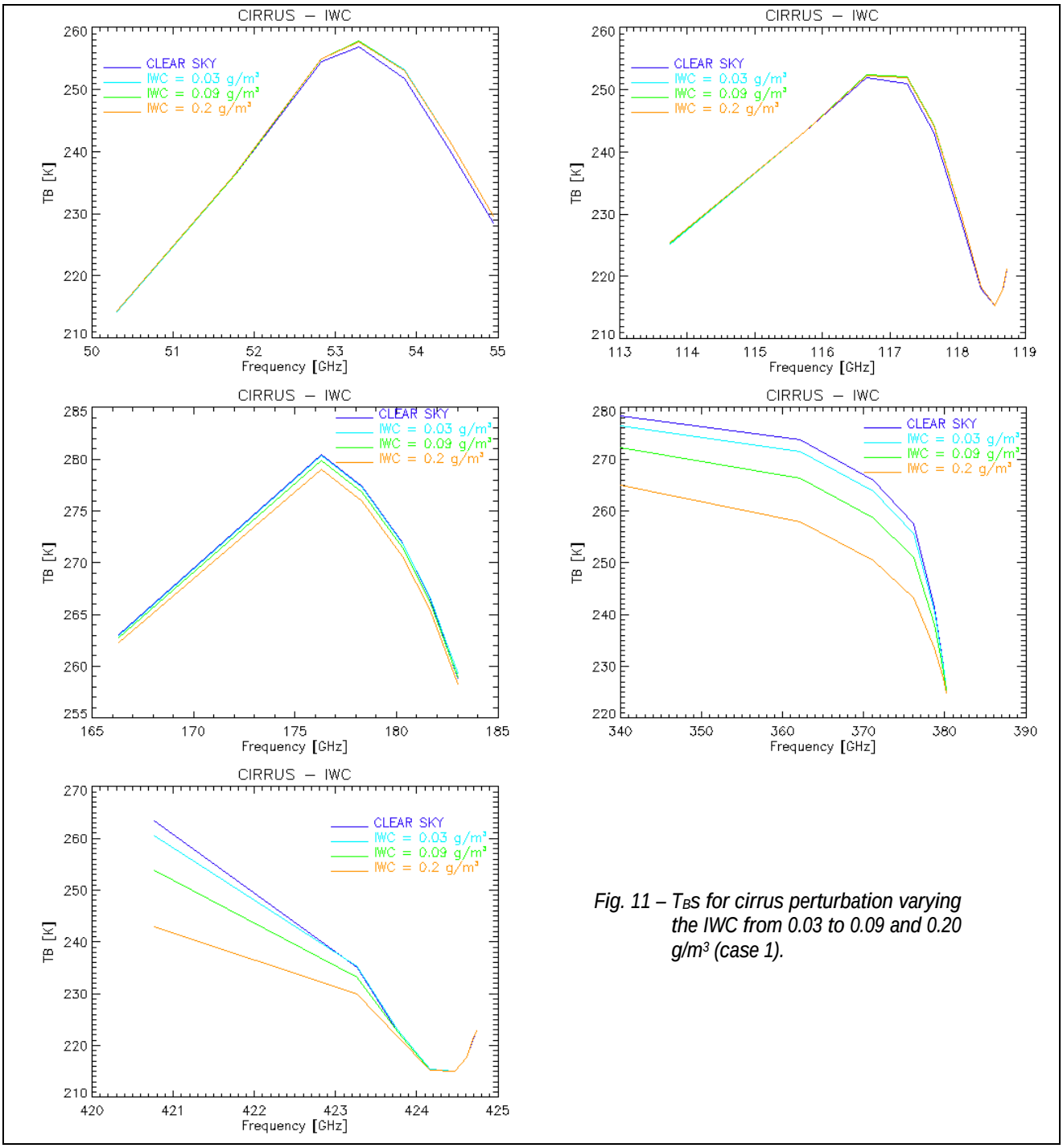

Fig. 11 – T_Bs for cirrus perturbation varying the IWC from 0.03 to 0.09 and 0.20 g/m³ (case 1).

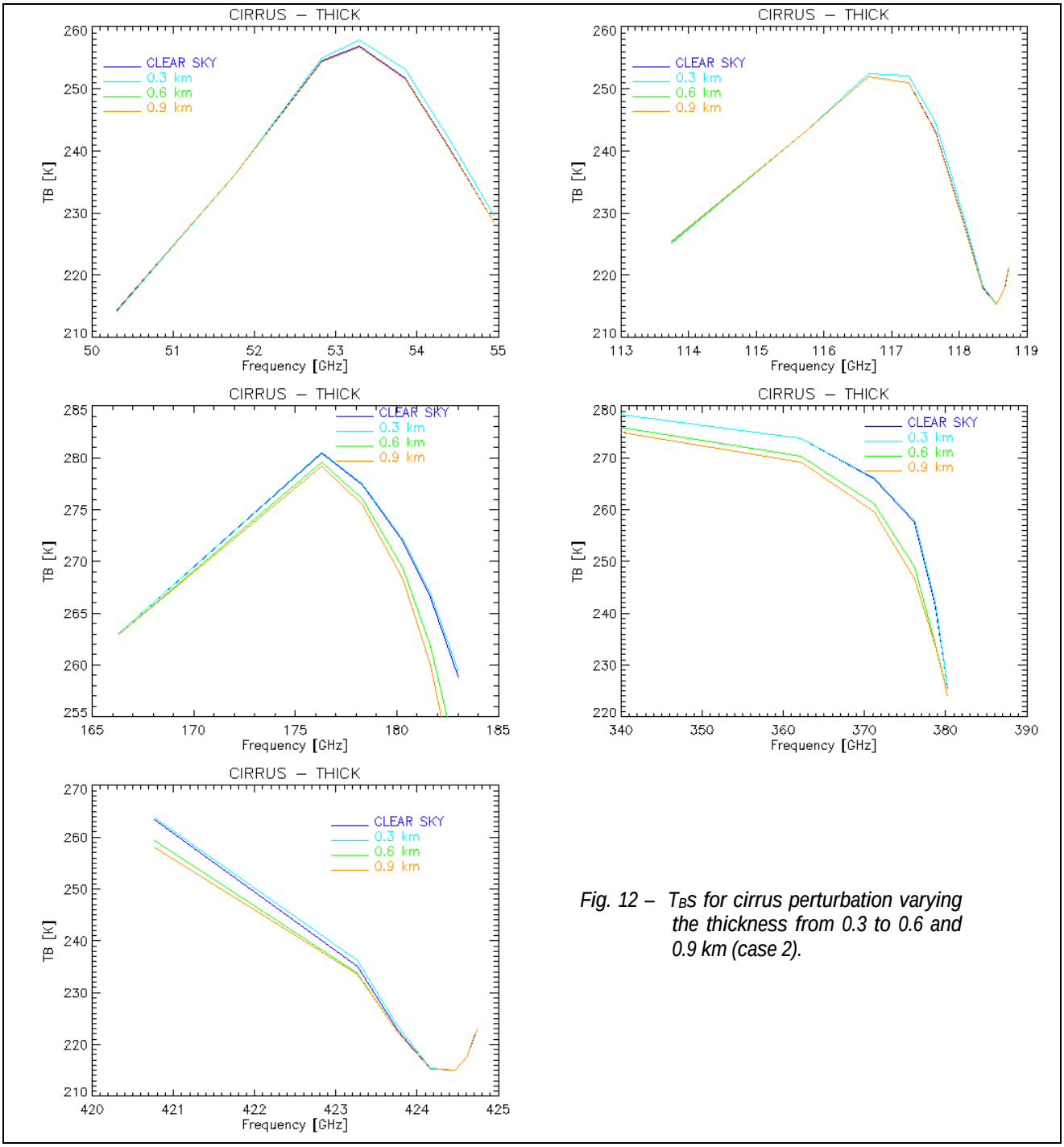

Fig. 12 – T_Bs for cirrus perturbation varying the thickness from 0.3 to 0.6 and 0.9 km (case 2).

5.2 Marine stratus

Fig. 13 and ***Fig. 14*** show the T_Bs of case 3 and case 4 respectively for every frequency grouped by bands. Fig. 13 refers to changes of LWC, Fig. 14 to variation of thickness. In this case, the most significant effect is the emission due to the liquid hydrometeors and the water vapour contained in the cloud at the lower frequencies (54, 118 and 183 GHz). The higher frequencies are almost insensitive to any variation of the LWC or water vapour content into the cloud.

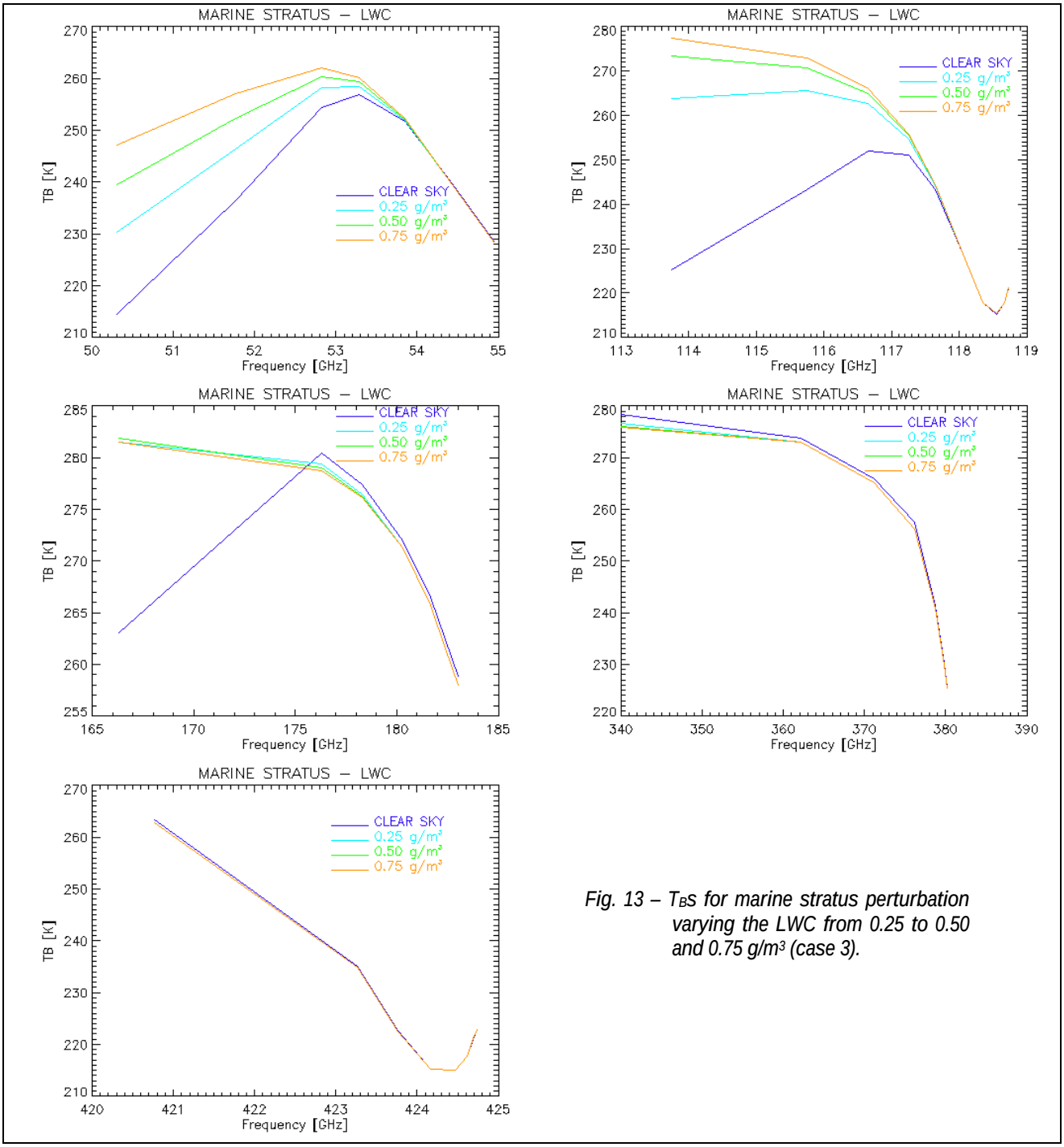

Fig. 13 – T_Bs for marine stratus perturbation varying the LWC from 0.25 to 0.50 and 0.75 g/m³ (case 3).

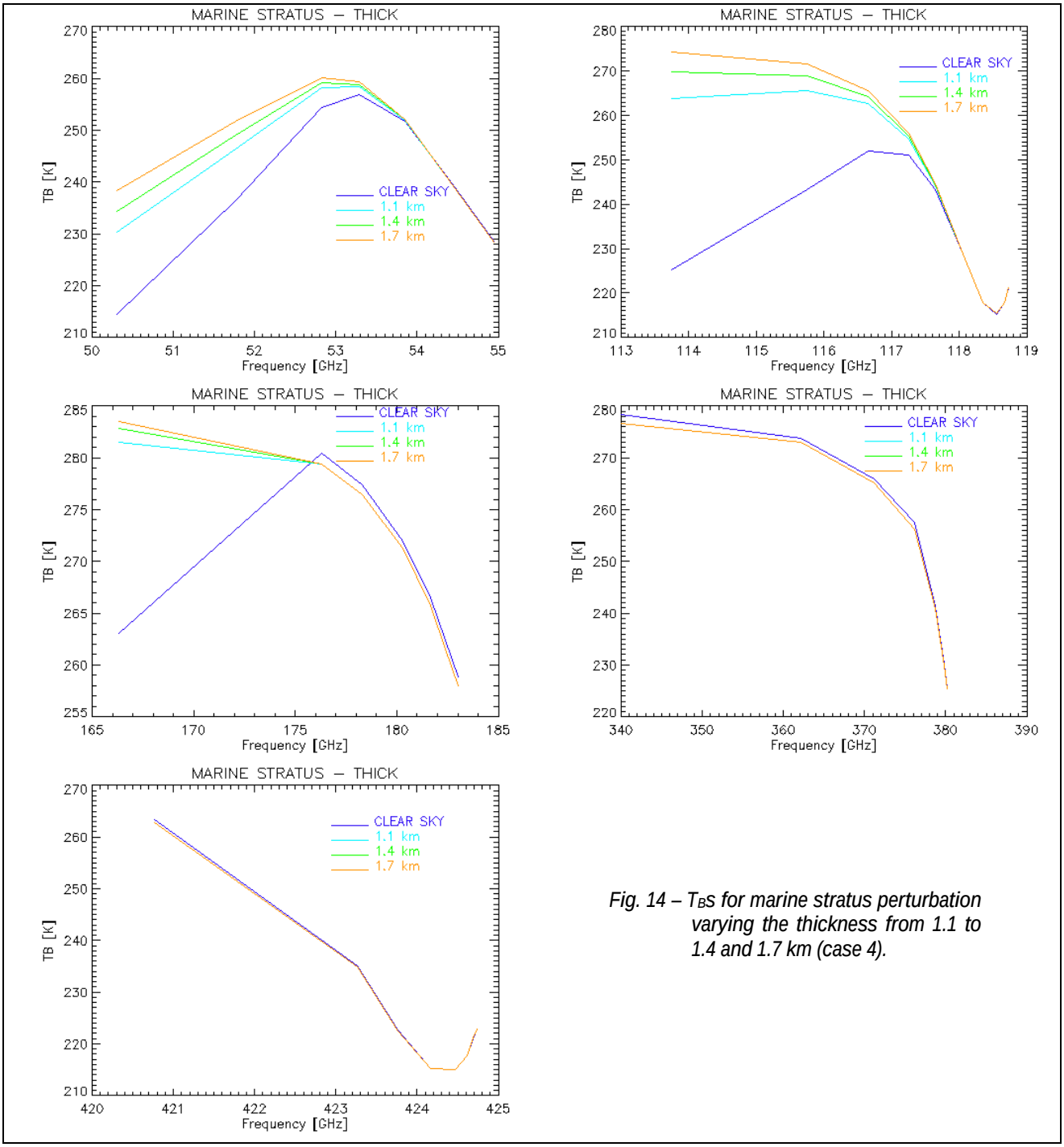

Fig. 14 – T_Bs for marine stratus perturbation varying the thickness from 1.1 to 1.4 and 1.7 km (case 4).

5.3 Nimbus-stratus

Fig. 15 and ***Fig. 16*** show the T_Bs of case 5 and case 6 respectively for every frequency grouped by bands. Fig. 15 refers to changes of LWC, Fig. 16 to variation of thickness. The higher frequencies (425 and 380 GHz) are less sensitive to both the LWC and the thickness variations, being able to distinguish between cloudy and clear sky. On the contrary, the lower frequencies (118 and 183 GHz) are both very sensitive in LWC and thickness variations.

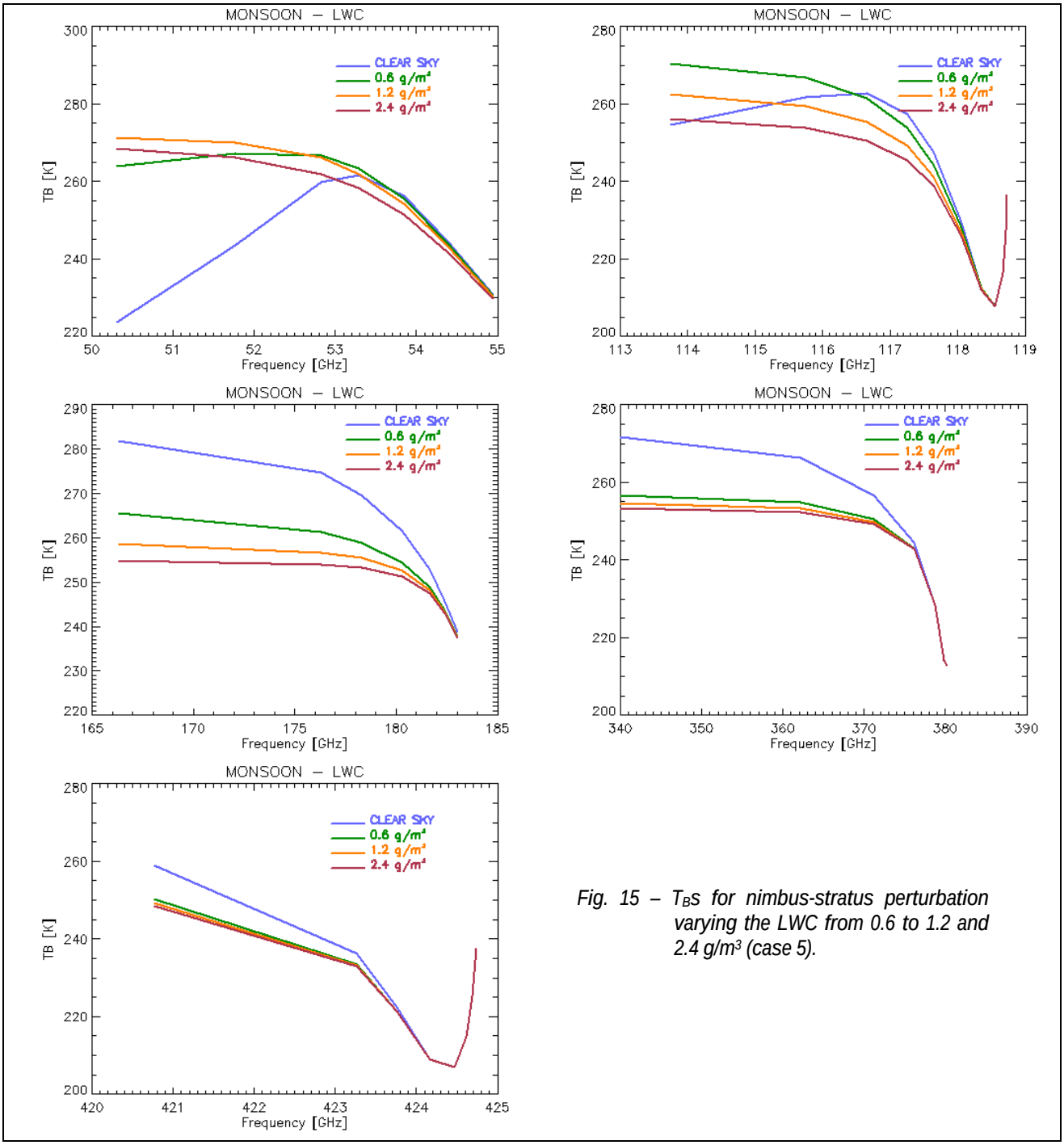

Fig. 15 – T_Bs for nimbus-stratus perturbation varying the LWC from 0.6 to 1.2 and 2.4 g/m³ (case 5).

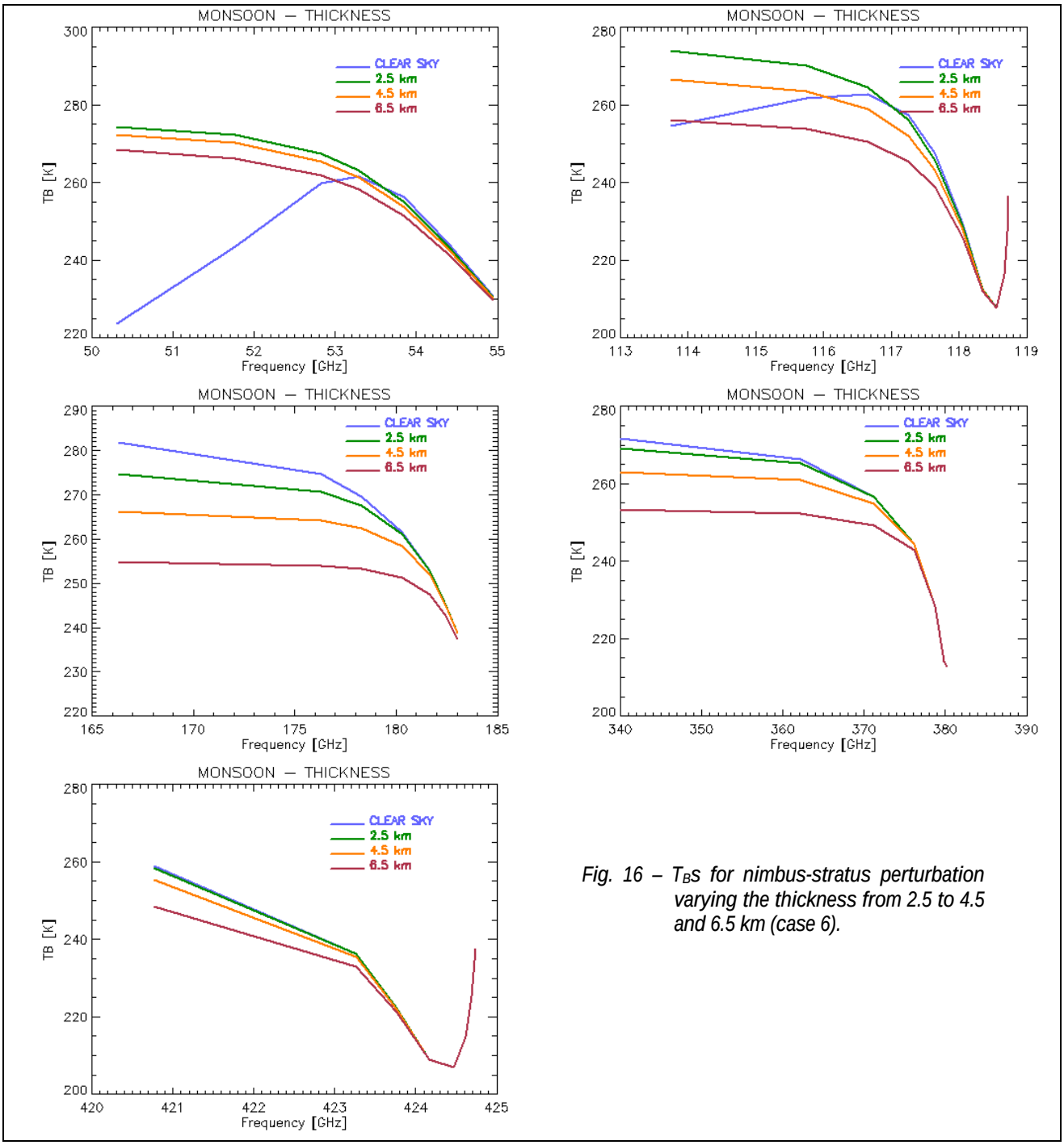

Fig. 16 – T_Bs for nimbus-stratus perturbation varying the thickness from 2.5 to 4.5 and 6.5 km (case 6).

5.4 Bands correlation

In ***Figures 17 to 22*** scatterplots are presented, of T_Bs of the 183 GHz v/s the 118 GHz band, and of the 380 GHz v/s the 425 GHz band, aimed at deploying how their sensitivity to differences of clear-air and cloudy conditions, and to changes of LWC or IWC and cloud thickness, are correlated.

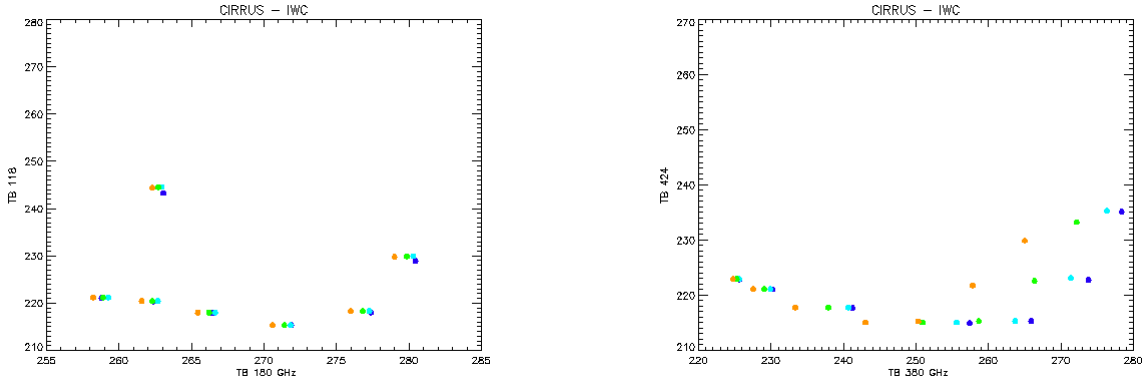

Fig. 17 – Scatterplots between two band association to retrieve water vapour in case 1 (cirrus with changing IWC). Left: 183 v/s 118 GHz; right: 380 v/s 425 GHz.

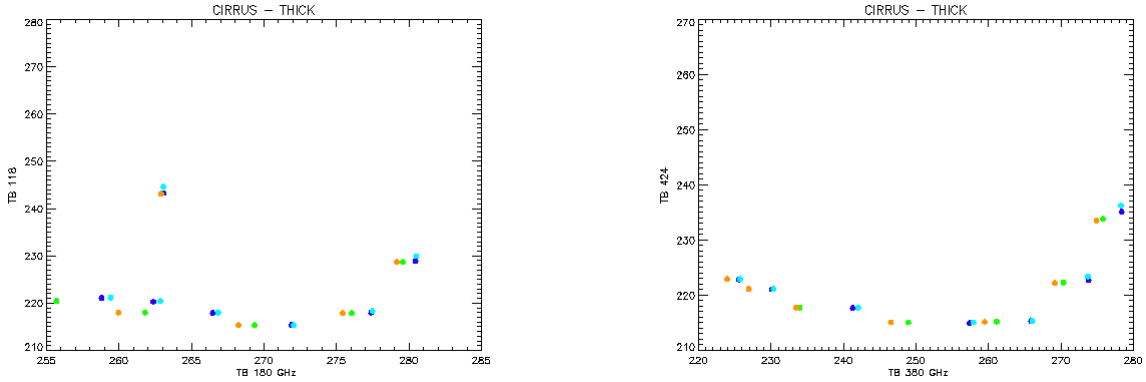

Fig. 18 - Scatterplots between two band association to retrieve water vapour in case 2 (cirrus with changing thickness). Left: 183 v/s 118 GHz; right: 380 v/s 425 GHz.

It is possible to see from Fig. 17 and Fig. 18 that, in the case of cirrus, the band couple 118+183 GHz is the less sensitive both to ice and ice thickness variation. It is easy to give an explanation if we consider that the scattering sensitivity to small ice particles becomes bigger with increasing frequencies.

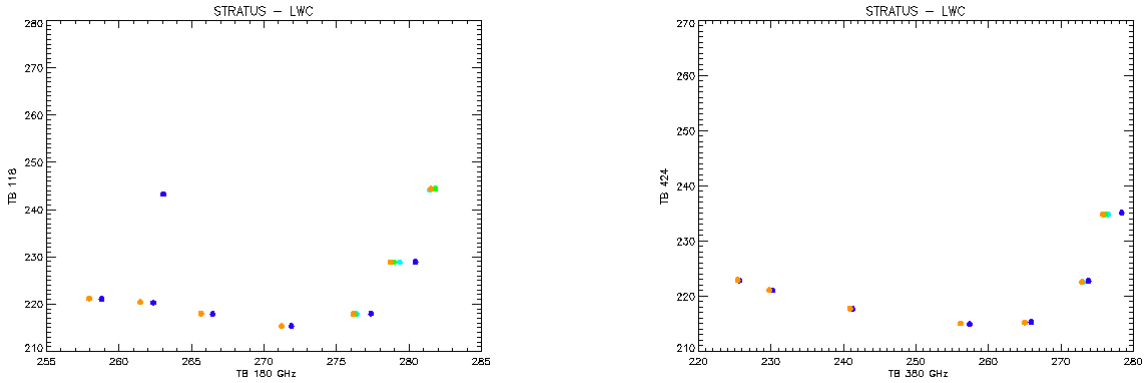

Fig. 19 – Scatterplots between two band association to retrieve water vapour in case 3 (maritime stratus with changing LWC). Left: 183 v/s 118 GHz; right: 380 v/s 424 GHz.

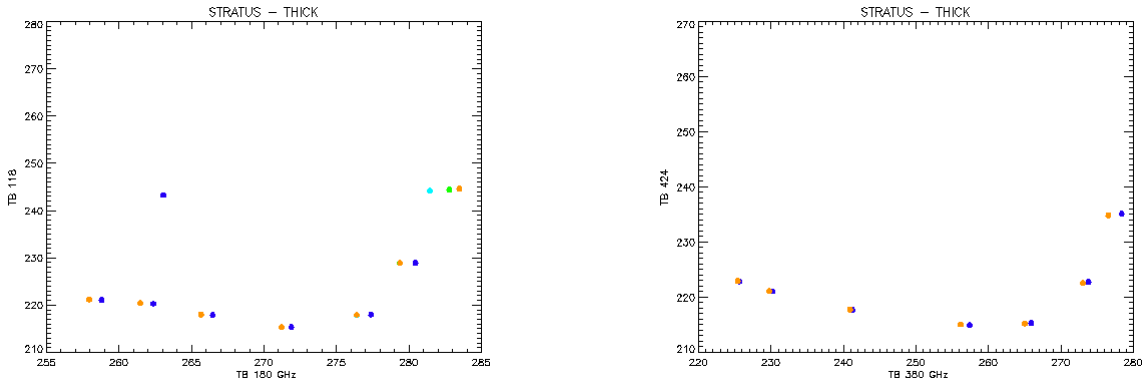

Fig. 20 - Scatterplots between two band association to retrieve water vapour in case 4 (maritime stratus with changing thickness). Left: 183 vs. 118 GHz; Right: 380 vs. 424 GHz.

The scatterplots for the marine stratus cases in Fig. 19 and Fig. 20 show that, opposite to the case of cirrus, the band couple 425+380 GHz is the most insensitive to LWC and cloud thickness variation. Also in this case we can consider that the emissivity effects are more intense at the lower frequencies.

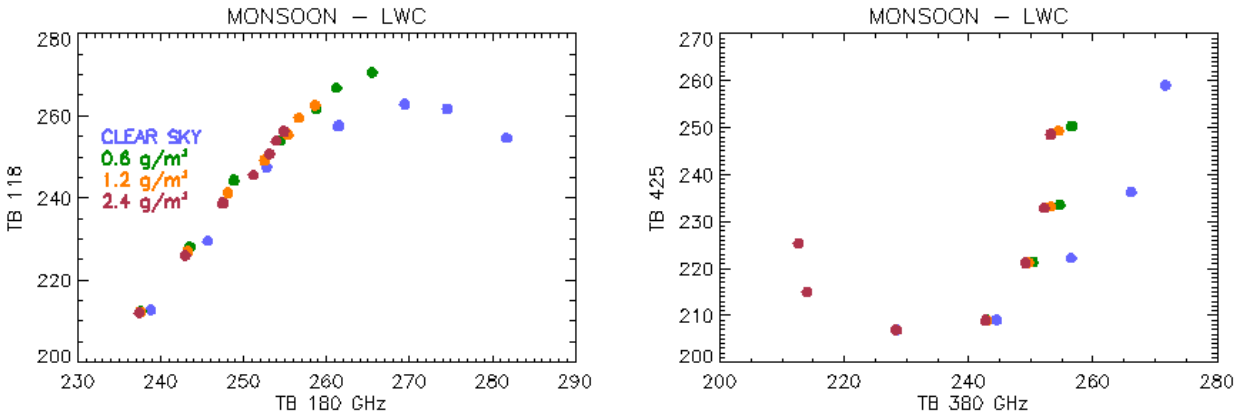

Fig. 21 – Scatterplots between two band association to retrieve water vapour in case 5 (nimbus-stratus with changing LWC). Left: 183 v/s 118 GHz; right: 380 v/s 425 GHz.

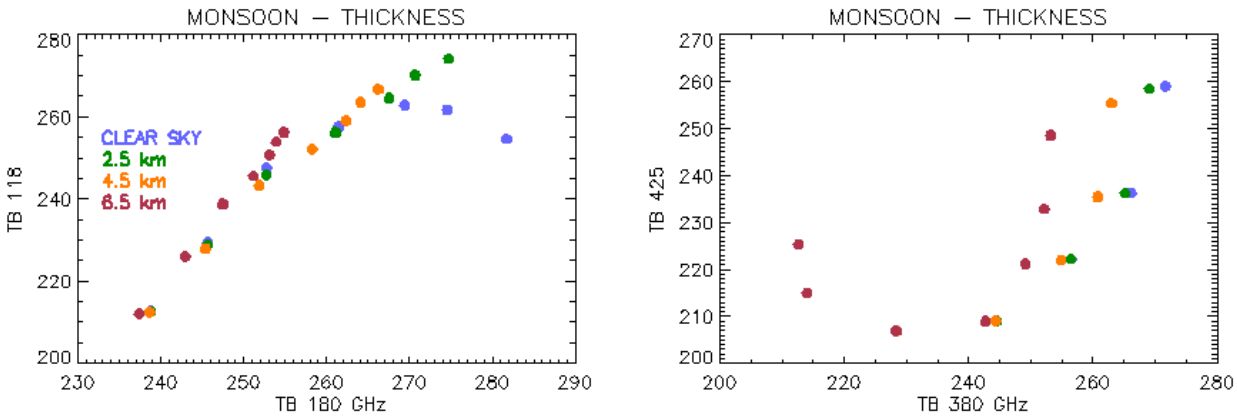

Fig. 22 – Scatterplots between two band association to retrieve water vapour in case 6 (nimbus-stratus with changing thickness). Left: 183 v/s 118 GHz; right: 380 v/s 425 GHz.

The scatterplots for nimbus-stratus (monsoon) in Fig. 21 and Fig. 22 show that the higher frequencies (380 and 424 GHz) seems to be more correlated, even if the weighting functions peaks in the middle troposphere.

6. Conclusions

In this study we have:

- assessed the temperature-humidity retrieval capability of GOMAS bands in clear-air;
- evaluated how profiles are perturbed by several types of cloud.

The results can be summarised as follows.

Clear-air profiling

- For temperature: profiles from the 54 GHz band are the most accurate up to near 300 hPa, then band 118 GHz becomes better. The 425 GHz band is obviously bad in the lower troposphere, but becomes the best above 250 hPa. The couple 54 + 118 GHz performs better than the couple 118 + 425 GHz up to about 350 hPa, whereas 118 + 425 prevails above. When using all three bands, an accuracy of about 1.5 K is achieved through a wide middle-high troposphere layer.
- For humidity: the profile from band 183 GHz (+118 GHz) performs better up to about 400 hPa whereas 340/380 + 425 GHz prevails above. When using both bands a performance of 5 % in the mid-troposphere is achieved.

Cloud perturbation

- Lower frequencies (54, 118 and 183 GHz bands) are not sensitive to variation of the IWC;
- High frequencies (380 and 425 GHz bands) are sensitive to variation of the IWC;
- There is weak or no sensitivity to cirrus thickness (except due to variation in water vapour profiles);
- The lower frequencies (54, 118 and 183 GHz bands) are sensitive to the emission from liquid hydrometeors and from the water vapour contained in the cloud;
- The higher frequencies (380 and 425 GHz bands) are almost insensitive to any variation of the LWC or water vapour content into the cloud;
- The band couple 118+183 GHz is the less sensitive both to IWC and ice thickness variation;
- The band couple 425+380 GHz is the most insensitive to LWC and cloud thickness variation.

All-weather profiling capability

Ii is not possible, by this relatively simple analysis, to directly reply to the question *how close to precipitating cores we can retrieve temperature-humidity profile*. In fact, it has been found that the performances of the different bands depend on the different cloud types considered. To reply to the direct question, it would be necessary to develop specific retrieval schemes for the different situations. The only thing that has been proven is that full sounding is possible in the presence of cirrus clouds by means of the lower frequency bands, 54, 118 and 183 GHz. In case of stratus, the advantage of high penetration of low-frequency bands is biased by higher sensitivity to liquid water and water vapour. On the contrary, in the presence of low clouds composed of liquid particles, the couple 425+380 GHz is the best choice, being very little sensitive to variation of water vapour and cloud LWC in the lower levels of the atmosphere.

Acknowledgements

We are in debit with:

- Philip Rosenkranz (MIT/RLE) for provision of the retrieval code utilised for the temperature-humidity clear-air experiment;
- Albin Gasiewski (NOAA/ETL) for provision of the MRT code utilised for the cloud perturbation experiment.

References

Bauer P., L. Schanz and L. Roberti, 1998: “Correction of the three-dimensional effects for passive microwave remote sensing of convective clouds”. *J. Appl. Meteor.*, 37, 1619-1632.

Bizzarri B. et al. (the 40 GOMAS proponents), 2002: “Requirements and perspectives for MW/sub-mm sounding from geostationary satellite”. *EUMETSAT Meteorological Satellite Conference*, Dublin, Ireland, 2-6 September 2002, 97-105.

Blackwell W.J. and D.H. Staelin, 1996: "Comparative performance analyses of passive microwave systems for tropospheric sounding of temperature and water vapor profiles". *GOES-8 and Beyond, Denver Co., August 7-9 1996 - SPIE Proceedings Series*, vol. 2812, 472-478.

Chedin A., Scott N.A., Wahiche C. and Moulinier P., 1985: “The improved intialization inversion method: A high resolution physical method for temperature retrievals from the TIROS-N series”. *J. Clim. Appl. Meteor.*, 24, 128-143.

Di Michele S., F.S. Marzano, A. Mugnai, A. Tassa and J.P.V. Poiares Baptista, 2003: “Physically-based statistical integration of TRMM microwave measurements for precipitation profiling”. *Radio Sci*., 38, 8072-8088.

Eyre J. R., 1989, “Inversion of cloudy satellite sounding radiances by nonlinear optimal estimation I: Theory and simulation for TOVS”, *Q. J. R. Meteorol. Soc.*, 115, 1101-1026.

Grody N.C., 1988: “Surface identification using satellite microwave radiometry”. *IEEE Trans. Geosci. Remote Sensing*, 26, 850-859.

Janssen M.A., 1993, “Atmospheric Remote Sensing by Microwave Radiometry”, New York, Wiley Ed..

Hewison T. and S. English, 2000: “Fast models for land surface emissivity”. *Radiative Transfer Models for Microwave Radiometry* (C. Matzler, ed.), COST Action 712, Directorate-General for Research, European Commission, Brussels, Belgium, 117-127.

Klein M. and A.J. Gasiewski, 2000: "The Sensitivity of Millimeter and Sub-millimeter Frequencies to Atmospheric Temperature and Water Vapor Variations". *J. Geophys. Res., Atmospheres*, vol. 13, p.17481-17511.

Kuo C.C. and D.H. Staelin, 1994: “Statistical Iterative Scheme for Estimating Atmospheric Relative Humidity Profiles”. *IEEE Trans. Geosci. Remote Sensing*, 32, 254-260.

Lamkaouchi K., Balana G.and Ellison W., 1997, “New Permittivity Data for Sea Water (30-200 GHz)”, *ESA Report* 11 197/94/NL/CN.

Liebe H.J. and G.G. Gimmestad, 1978: “Calculation of clear air EHF refractivity”. *Radio Sci*., 13, 245-251.

Liebe H.J., 1985: “An updated model for millimeter wave propagation in moist air”. *Radio Sci*., 20, 1069-1089.

Liu Q., C. Simmer and E. Ruprecht, 1996: “Three-dimensional radiative transfer effects of clouds in the microwave spectral range”. *J. Geophys. Res*., 101, 4289-4298.

Mugnai A., S. Di Michele, F.S. Marzano and A. Tassa, 2001: “Cloud-model based Bayesian techniques for precipitation profile retrieval from TRMM microwave sensors”. *ECMWF/EuroTRMM Workshop on Assimilation of Clouds and Precipitation*, ECMWF, Reading, U.K., 323-345.

Roberti L., J. Haferman and C. Kummerow, 1994: “Microwave radiative transfer through horizontally inhomogeneous precipitating clouds”. *J. Geophys. Res*., 99, 16707-16718.

Rodgers C.D., 1976: “Retrieval of atmospheric temperature and composition from remote measurements of thermal radiation”, *Rev. Geophys. and Space Phys.*, 14, 609-624.

Rogers R.R. and M.K. Yau, 1996: “*A Short Course in Cloud Physics*”. Butterworth-Heinemann, pp 290.

Rosenkranz P.W., 1995: “A rapid atmospheric transmittance algorithm for microwave sounding channels”. *IEEE Trans. Geosci. Remote Sensing*, 33, 1135–1140.

Rosenkranz P.W., 1998: “Improved rapid transmittance algorithm for microwave sounding channels”. In *1998 IEEE Int. Geoscience and Remote Sensing Symp.Proc.*, 728–730.

Rosenkranz P.W., 2001: “Retrieval of temperature and moisture profiles from AMSU-A and AMSU-B measurements”. *IEEE Trans. Geosci. Remote Sensing*, 39, 2429-2435.

Shaw R.A, 2003: “Particle-turbulence interactions in atmospheric clouds”. *Annual Review of Fluid Mechanics*, Vol. 35: 183-227, 2003.

Sundvquist H., Berge H., and Kristjansson, 1989, “ Condensation and cloud studies with a mesoscale numerical prediction model”, *Mon. Wea. Rev.*, 117, 1641-1657.

Tassa A., S. Di Michele, A. Mugnai, FS. Marzano and J.P.V. Poiares Baptista, 2003: “Cloud-model based Bayesian technique for precipitation profile retrieval from TRMM Microwave Imager”. *Radio Sci*., 38, 8074-8086.

Telford J.W. and P.B. Wagner, 1981: “Observations of condensation growth determined by entity type mixing”. *Pure & Appl. Geophys*., 119, 934-965.

Wang J.R. and L.A. Chang, 1990: “Retrieval of water vapor profiles from microwave radiometric measurements near 90 and 183 GHz”. *J. of App. Meteor*., 29, 1005-1013.

Wang P.K.H, 2005: “Assessment of Precipitation Characters between Ocean and Coast area during Winter Monsoon in Taiwan”. *Proceeding of International TOVS Study Conferences - XIV*, Beijing, China, 25-31 May 2005.

Wilheit T. T., 1990 “An algorithm of retrieving water vapor profiles in clear and cloudy atmospheres from 183 GHz radiometric measurements, Simulation studies” *J. of App. Meteor*., 29, 508-515.

Wilheit T. T. and K.D. Hutchinson, 1997: “Water vapor profiles retrievals from SSM/T-2 data constrained by infrared – based cloud parameters ” *Int. J. Remote Sensing*, 18, 3263-3277.

Acronyms

AIRS	Atmospheric Infrared Sounder
AMSU	Advanced Microwave Sounding Unit (on NOAA and MetOp)
AMSU-A	Advanced Microwave Sounding Unit - A (on NOAA, MetOp and EOS-Aqua)
AMSU-B	Advanced Microwave Sounding Unit - B (on NOAA up to NOAA-17)
CNR	Consiglio Nazionale delle Ricerche
ETL	Environmental Technology Laboratory (of NOAA)
GAIRS	Geostationary AIRS
GEM	Geostationary Microwave Observatory
GEO	Geostationary Earth Orbit
GOMAS	Geostationary Observatory for Microwave Atmospheric Sounding
IASI	Infrared Atmospheric Sounding Interferometer (on MetOp)
IFOV	Instantaneous Field Of View
ISAC	Istituto di Scienze dell'Atmosfera e del Clima (of CNR)
IWC	Ice Water Content
IWF	Incremental Weighting Function
LWC	Liquid Water Content
MHS	Microwave Humidity Sounder (on MetOp and NOAA-18/19)
MIT	Massachusetts Institute of Technology
MRT	Microwave Radiative Transfer
MW	Microwave
NEΔT	Noise-Equivalent Differential Temperature
NOAA	National Oceanographic and Atmospheric Administration (of USA)
NWP	Numerical Weather Prediction
RLE	Research Laboratory of Electronics (of MIT)
RTE	Radiative Transfer Equation
RTM	Radiative Transfer Model
s.s.p.	Sub-satellite-point
SNR	Signal-to-Noise Ratio
T_B	Brightness temperature
TIGR	Thermodynamic Initial Guess Retrieval